Letters on Materials 12 (4s), 2022 pp. 463-468 www.lettersonmaterials.com

https://doi.org/10.22226/2410-3535-2022-4-463-468

Check for updates

Effect of HPT straining and further natural aging on the structure and hardness of aluminum alloy 1965 with nanosized TM aluminides

M. V. Markushev†, E. V. Avtokratova, S. V. Krymskiy, V. V. Tereshkin, O. Sh. Sitdikov

†mvmark@imsp.ru

Institute for Metals Superplasticity Problems, RAS, Ufa, 450001, Russia

Pre-quenched samples cut from a homogenized ingot of commercial aluminum alloy 1965 with a grain size of about 21 μm were compressed at 6 GPa and then strained by torsion up to 10 revolutions at room temperature. TEM, SEM and XRD analyses showed that the strengthening/softening of the alloy during further natural aging up to 500 hrs was controlled by simultaneous decomposition of the aluminum solid solution and recovery of its deformation structure. It was found that the two-level nanostructuring of the alloy (precipitates and matrix) is accompanied by more than twofold strengthening up to a hardness of about 250 HV. The main contribution was made by dislocation and structural hardening due to the formation of a highly work-hardened structure of the nanofragmented type. During subsequent aging, the change in hardness was controlled by both the preliminary strain and the aging time. A continuous increase in strength with strain and aging time was found in the samples after pressing and torsion up to 1 revolution. In other conditions, strengthening was preceded by softening, the magnitude and duration of which were also proportional to the strain. The nature of the alloy behavior and the role of nanosized aluminides of transition metals are discussed in details.

Keywords: high-strength aluminum alloy, high pressure torsion, natural aging, strength.

1. Introduction

It is known that "cold" severe plastic deformation (SPD) of aluminum alloys commonly leads to the formation of a fragmented non-equilibrium nanostructure with crystallite (grain and sub-grain) sizes less than 0.5 μm and a high dislocation density [1–4]. Billets with such a structure usually exhibit abnormally high strength and critically low ductility under static loading at ambient temperature [1–6]. However, a rational and even unique balance of mechanical properties can be obtained by SPD at elevated temperatures [3,7] or by a complex thermomechanical treatment involving prior- and/or post-SPD heat treatment [2,3,8,9]. The general approach of such a treatment is aimed at imparting a more equilibrium nanostructure of the grain type. Namely, it is often recommended to obtain partially or completely recovered/recrystallized structures with equiaxed crystallites separated by predominantly high-angle boundaries, or at least with an increased mean angle of their misorientations [8,10]. However, a simultaneous and significant increase in ductility and durability of the SPD-processed material, due to an increase in its toughness and crack resistance under subsequent heat treatment, usually resulted in a significant loss of the work-hardening effect and, consequently, in a decrease in the strength parameters [2,4,10,11]. To overcome this situation, analysis of the potential of the technological route that realizes a dual strengthening effect due to both SPD and post-SPD heat treatment is of great importance, especially for high-strength aluminum alloys.

In this connection, the present study is aimed at an investigation of the effects of the SPD, realized by high-pressure torsion (HPT), and the time of further natural (at ambient temperature) aging on the kinetics and hardening/softening level of the modern high-strength aluminum alloy with complex additions of transition metals (TM).

2. Material and procedure

Disk-shaped samples 20 mm in diameter and 2 mm thick, cut out from the homogenized ingot of a commercial alloy 1965 (Al-8.1Zn-2.3Cu-0.27Sc-0.10Zr-0.10Mn), were solution treated at 460°C and quenched in water. Further SPD was realized immediately via room temperature HPT under a pressure of 6 GPa and in the range of 0.1 to 10 revolutions. Some of the samples were compressed in the HPT tool without any rotation. Post-SPD aging was carried out at a room temperature with exposure up to 500 hrs.

The alloy structure was analyzed at half the radius of the sample by scanning and transmission electron microscopy (SEM and TEM) and X-ray diffractometry. The latter was performed in the Cu-K_α radiation with a wavelength λ =1.54418 Å on a DRON-4-07 device operated at 40 kV and 30 mA current, with rotated sample, 4 sec scanning with a step of 0.1°, and a graphite monochromator on the diffracted beam. The root-mean-square microstrain of the crystal lattice ($<\varepsilon^2>^{1/2}$) and the coherent domain size (CDS) were calculated by the full-profile method using MAUD software. Deviations of the measurements did not

exceed 0.001% and 5 nm, respectively. Dislocation density, ρ, was calculated as:

$$\rho = 2\sqrt{3}\left\langle \varepsilon^2 \right\rangle^{\frac{1}{2}} / \left(D_{CDS} \times b \right),$$

where b is the Burger's vector. SEM and TEM analyses were carried out using MIRA TESCAN and JEOL 2000EX microscopes, respectively. Objects were prepared by jet-electro-polishing at a current of 20 V and temperature of −28°C on the Tenupol 5 unit in a solution of 750 ml CH_3OH and 250 ml HNO_3. The mean sizes of crystallites and precipitates were evaluated from the equivalent diameter with a measurement error of less than 10% and using computer image analysis.

Microhardness (HV) was determined using ITV-1-M tester at the load of 1 N and 15 sec exposure. Ten measurements on a point at half the radius of the sample were performed to obtain an error below 5%.

3. Results and discussion

The alloy microstructure in the pre-quenched state consisted of equiaxed 21 μm grains and about 4% of coarse excess phases of different size and composition (more details in [12,13]), preferably located in grain boundary areas (Fig. 1a). As a result of homogenization, the alloy matrix was dispersion strengthened by the products of decomposition of aluminum solid solution, abnormally saturated by TM during casting. These precipitates of $Al_3(Zr, Sc)$-phases (so-called dispersoids), were preferably coherent with the aluminum matrix (Figs. 1b, c) and nanosized [14,15].

Basing on the qualitative and quantitative changes in the parameters and structure type during deformation (Figs. 2 and 3), three main stages of the alloy behavior can be suggested. Even after pressing to 20% and compression for 1 min at 6 GPa, recognized as a first stage, an almost three-order of magnitude increase in the dislocation density was observed (Fig. 3) with no visible changes in the geometry of the initial grains (Fig. 2 a). It was supported by about three-fold refinement of coherent domains and growth of internal stresses to maximum values (Fig. 3). Such evolution of the structure resulted in an increase in the alloy hardness by about 35 HV (Fig. 4).

Thus, the first processing stage involving only high pressure of the samples had a high impact in the alloy work-hardening. TEM observations showed that this effect was conditioned by extremely homogeneous distribution of high dislocation densities inside the initial grains and their boundaries without the formation of conventionally observed work-hardened structures with dislocation walls, deformation bands and cells subdividing the grains. Besides, the strong increase in lattice defectiveness led to a sharp decrease in the CDS with only a few degree misorientations, as well as to a sharp increase in the internal stresses and the aluminum lattice parameter (Fig. 3). The observation of changes in the first two parameters was quite reasonable and expectable. However, the lattice parameter evolution was quite unusual. Obviously, it could be a consequence of changes in two factors — the dislocation densities, and the alloying of the solid solution. The latter could be due to: a) well-known incompleteness of homogenization of the cast structure, which is commonly detected by the decrease in the fraction and size of excess phases; b) dissolution of dispersoids or c) decomposition of the solid solution with the formation of zones containing Zn, Mg and Cu. Among the alloying elements involving TM, only Mg is capable to increase the Al lattice parameter [16]. Thus, the strain-induced dissolution of phases, having cast origin and containing Mg, could be the sources of the found alloy behavior. However, our previous investigations [12–14,17] showed no sense dynamic dissolution of excess phases up to 10 revolutions. During HPT there was a decrease in their size via mechanical failure, which was supported by fraction reductions, not exceeding 0.5%. Thus, it should be stated that the increase in the aluminum lattice parameter after applying high pressure could be caused by an increase in its defectiveness, registered by three-order of magnitude increase in the density of dislocations.

The application of 0.1 revolution revealed the second stage of processing, which resulted in the formation of a well-defined cell structure with distinct dense dislocation walls (Fig. 2), while integral dislocation density remained close to the compressed one (Fig. 3). This stage prolonged until 1 turn, during which a rearrangement of the dislocation/cell structure was observed, activated by more than 50% increase in dislocation density. Along with higher dislocation density and homogeneity, the structure processed was characterized by more misoriented domains (Figs. 2 b – e). These factors resulted in a more pronounced alloy deformation strengthening, exceeding 50 HV, in spite of minimum changes in other structure parameters.

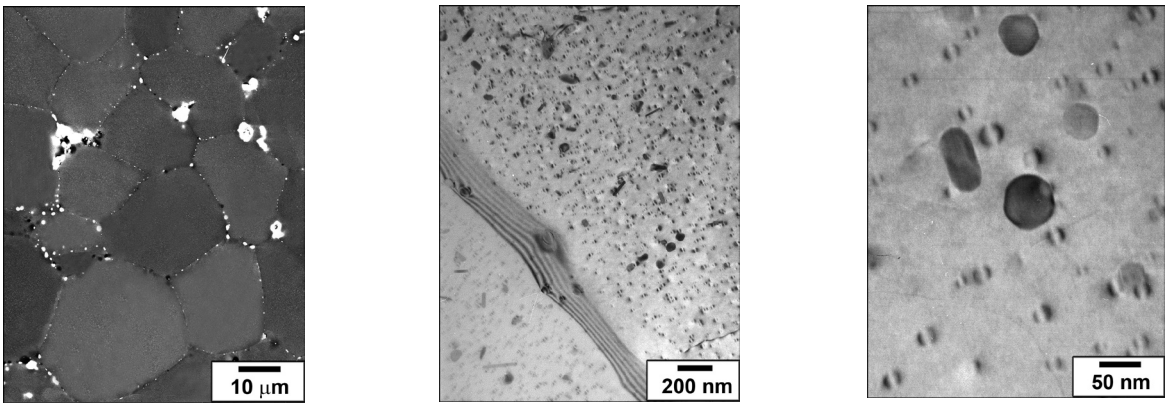

a b c

Fig. 1. SEM (a) and TEM (b, c) structures of the cast alloy 1965 after quenching.

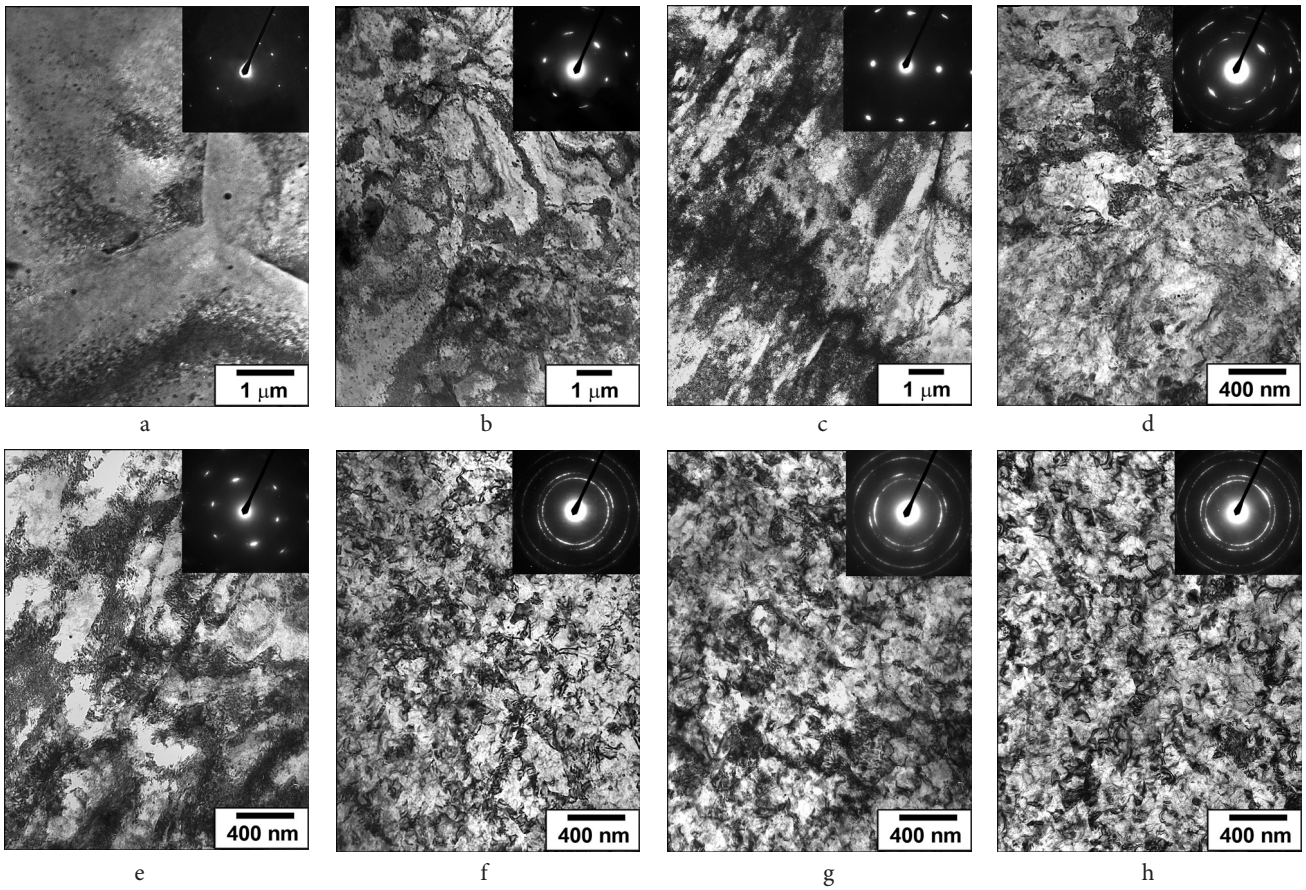

Fig. 2. TEM structures and SAED patterns for the 1965 alloy after compression (a) and further HPT to 0.1 (b), 0.3 (c), 0.5 (d), 1 (e), 2 (f), 5 (g) and 10 (h) rotations.

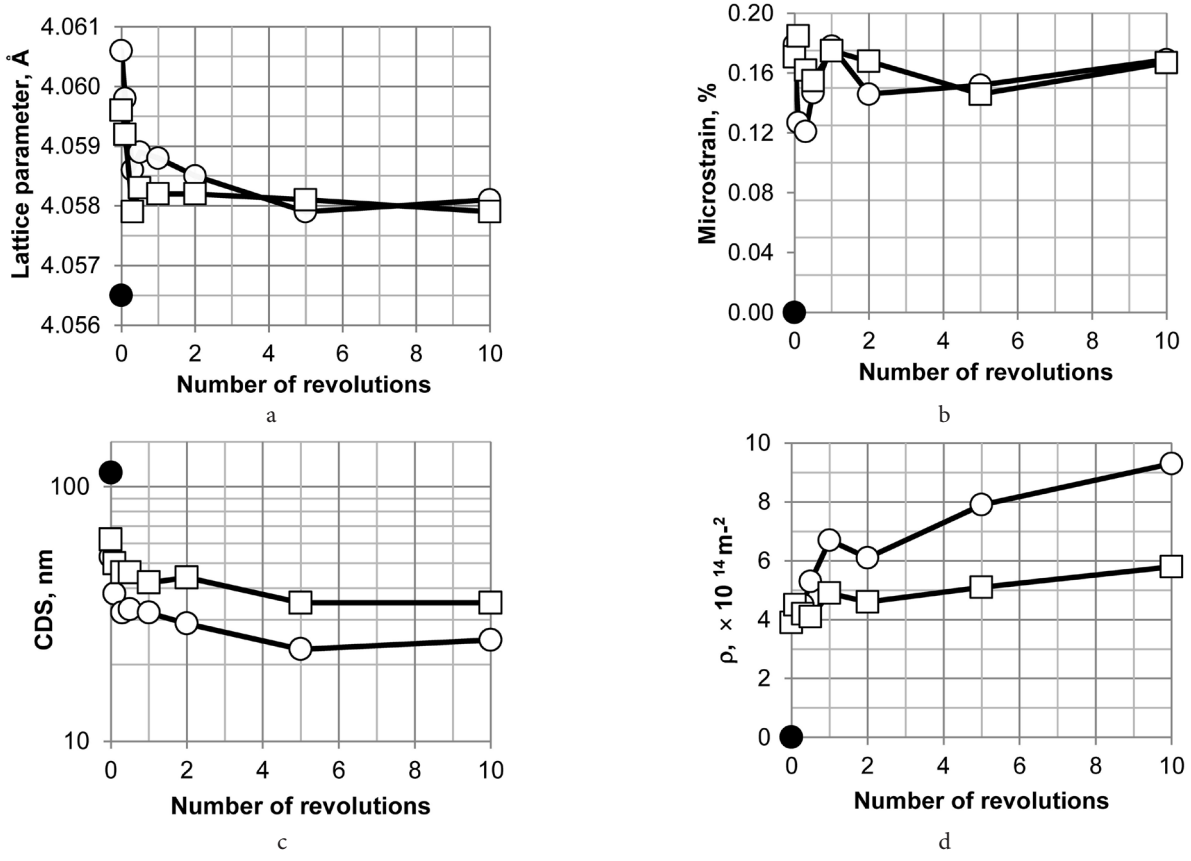

Fig. 3. Dependences of lattice parameter (a) and root-mean-square microstraining (b), coherent domain size (c) and integral dislocation density (d) vs number of revolutions under HPT for the 1965 alloy after deformation (○) and further natural aging (□). (●) corresponds to the values in the pre-quenched alloy.

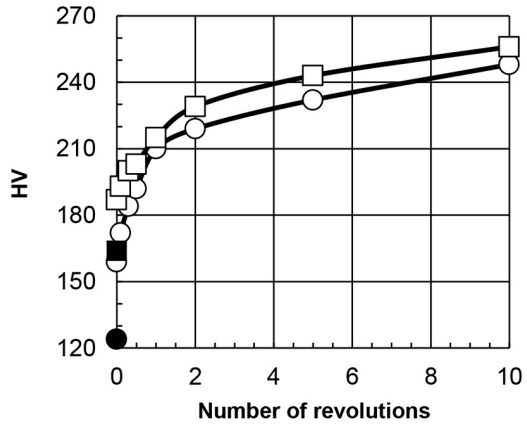

Fig. 4. Dependences of hardness (HV) on strain for the 1965 alloy after HPT (○) and subsequent natural aging (□). (●) and (■) correspond to the hardness of cast pre-quenched and naturally aged alloy, consequently.

Under further straining at the third stage, being observed up to 10 rotations, the structure got another quality via transformation into the well-developed, non-equilibrium nanofragmented one with an average size of near equiaxed crystallites (grains and subgrains) of about 100 nm (Figs. 2 f – h). First of all, this stage is evident from the changes in the selected area electron diffraction (SAED) patterns in Fig. 2. It can be seen that after the pressing the reflections still indicate the presence of coarse-grain structure. On the second stage, torsion even to 0.1 revolutions led to the formation of the point-wise reflections from some areas of crystallites mostly surrounded by low-angle boundaries. With further straining to 1 turn, the reflections tended to stretch azimuthally and to 2 turns transformed into the Debye rings, suggesting the development of more misoriented and fine (sub)structures. Judging to the character features of structure developed it could be concluded that fragmentation (subdivision) and continuous dynamic recrystallization [18,19] played the dominant role in its formation.

As seen in Fig. 2, dispersoids were also currently visible through all stages of deformation processing, starting from pressing, in spite of too complex TEM contrast. Meanwhile, note that their distinct number and fraction estimation from TEM pictures is impossible. Moreover, the concurrent dynamic decomposition of preliminary oversaturated by main alloying elements aluminum solid solution under quenching was also not revealed. It was conditioned by low resolution of TEM used to receive the pictures from the products of dynamic aging less than nanometer in size, and also due to the mentioned complex contrast from the surrounded highly defected aluminum matrix. Therewith, basing on the data of the present microstructure analysis, it is impossible to declare the right observation of even the partial strain induced dissolution of the TM aluminides under HPT, which was observed in few studies (for instance, in [20, 21]). And also impossible to talk about the strain induced aging with formation of clusters and zones.

It could also be considered that HPT involving the first two stages, that is, to only one rotation, had a dominant impact on the alloy work-hardening and resulted in the alloy hardness close to 85% of the maximum value measured in the present study. It is also important to note that this strong alloy strengthening was conditioned by the formation of a homogeneous low misoriented dislocation wall/cell structure only. One of the major roles in its development was virtually played by dispersoids, which prevented dislocation glide and their rearrangement over long distances. The formation of bulk structures, frequently described as dense dislocation walls, was the main character of the structure at these HPT stages.

The aging response of the alloy in the states studied revealed two types of their behavior (Fig. 5). In the non-deformed initial alloy, as well as in the samples subjected to compression and then to torsion up to 1 revolution, their hardness continuously increased with the HPT strain and the duration of annealing. This behavior could only be explained by the alloy zone aging, which is described in [22, 23] and represented in Fig. 5 for the non-deformed

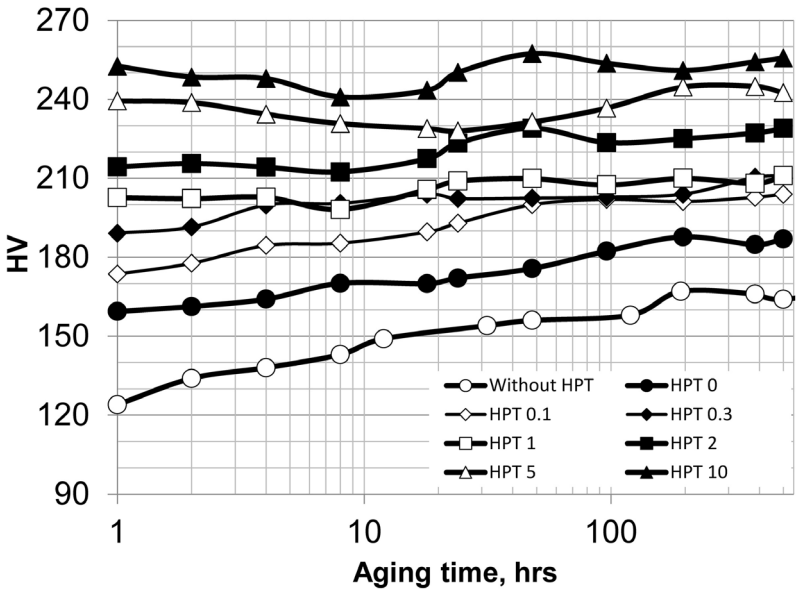

Fig. 5. Kinetics of the 1965 alloy room temperature aging before and after HPT to different strains. HPT 0 – 10 correspond to the conditions after compression and number of rotations, consequently.

initial cast condition. Under other conditions, hardening was preceded by a slight softening, whose value and time were also proportional to the HPT strain. It should be noted that this behavior showed an actual character of a severely deformed and nanostructured alloy. After 500 hrs of exposure at ambient temperature, their hardness returned to the values of the consequent HPT- processed conditions.

Therewith, the kinetics and magnitude of the age-hardening effect in the severely deformed alloy depend on the parameters of the (nano)structure of the matrix formed. The maximum age hardening was observed when the initial structure was dislocation/cellular in origin (Fig. 4). With the transition to a more misoriented nanofragmented structure due to HPT, the zone hardening proceeded along with the softening caused by the matrix structure recovery. The latter is evident from the decrease in dislocation density, internal stresses, and increase in coherent domain size (Fig. 3). Thus, natural aging after HPT up to 1 turn resulted in continuous hardening of the alloy. At higher rotations, aging in the early stages (up to 20 hrs) led to softening of the alloy due to prevailed static recovery, which could probably eliminate the effect of zone aging via dissolution of clusters by moving dislocations. And when the structure of the matrix acquired the features of the recovered one, the aging effect was also returned and compensated the hardness up to the HPT-ed alloy level. As a result, an abnormally high hardness of about 250 – 260 HV after the alloy processing to 10 revolutions restored and looked stable due to the combination of three strengthening effects in one processing route — disperse strengthening on nanosized precipitates of TM aluminides due to prior heat treatment, structural strengthening owing to deformation nanostructuring of matrix at HPT, and zone hardening at post-SPD natural aging.

However, it should be pointed out that the effect of the alloy age-hardening reduced with strain (Fig. 5). The origin is virtually based on the response of different types of severely deformed structures to static recovery at aging. Thus, compared to the dislocation/cellular structure, the fragmented one demonstrates much more intense recovery. It followed from the higher decrease in dislocation density due to aging (Fig. 3), which could be the only cause of the mentioned difference in the alloy behavior found.

Three other facts can also be emphasized. First, the HPT-ed alloy in the range of 0.1–1 revolutions gained the same hardness due to aging. Second, as discussed above, the maximum strengthening intensity of the alloy was observed at straining with low (up to 2 rotations) strains. And further aging gave the alloy hardness of about 210 – 230 HV, which is only 10 –15% less than the maximum level found in the present study. Third, the hardness of the alloy after HPT up to 5 and 10 revolutions as a result of natural aging became almost equal. So, it could be concluded, that in terms of achieving an effective strengthening of the alloy due to SPD, the latter should be limited by the formation of homogeneous low misoriented dislocation wall/cellular structure.

4. Conclusions

A room temperature HPT at 6 GPa up to one revolution only had a dominant effect on the work-hardening of the high-strength aluminum alloy 1965 and resulted in its hardness approaching almost 85% of the value obtained after 10 revolutions. Such strengthening of the alloy was due to the formation of a homogeneous low-misoriented dense dislocation-/cellular nanostructure. One of the main roles in its development was played by the high densities of nanosized TM aluminides, which prevent dynamic recovery by limiting the long-range glide of lattice dislocations and their rearrangement with the formation of planar-boundary structures.

With subsequent natural aging up to 500 hours, the change in the hardness of the alloy was within the range of 30 HV and was controlled by both HPT strain and aging time. In the pressed and torsioned to 1 revolution alloy, aging resulted in a continuous increase in strength. Further straining also led to hardening, but it was preceded by softening, the magnitude and duration of which were also proportional to number of rotations. As a result, the alloy subjected to HPT in the range of 0.1–1 revolutions and subsequent natural aging gained the same hardness of about 210 HV, while the hardness after HPT up to 5 and 10 revolutions and aging became practically equal to about 250 HV.

Acknowledgments. The work was supported by the Ministry of Science and Higher Education of Russian Federation through the state assignment of IMSP RAS on the basis of Shared Service Center of IMSP RAS "Structural and Physics-Mechanical Studies of Materials" (AAAA-1919- 119021390107-8).

References

1. R. R. Mulyukov, R. M. Imayev, A. A. Nazarov, M. F. Imayev, V. M. Imayev. Superplasticity of Ultrafine Grained Alloys: Experiment, Theory, Technologies. Nauka, Moscow (2014) 284 p. (in Russian)
2. M. V. Markushev. In: Perspektivnye Materialy. Vol. 8 (ed. by D. L. Merson). TSU Press, Togliatti, Russia (2019) p. 227. (in Russian)
3. M. V. Markushev, A. Vinogradov. In: Severe Plastic Deformation: Towards Bulk Production of Nanostructured Materials (ed. by B. Altan). Nova Science Publishers, USA (2006) 233 p.
4. Y. Estrin, A. Vinogradov. Acta Mater. 61, 782 (2013). Crossref
5. T. G. Langdon. Acta Mater. 61, 7035 (2013). Crossref
6. I. A. Ovid'ko, R. Z. Valiev, Y. T. Zhu. Progr. Mater. Sci. 94, 462 (2018). Crossref
7. I. Sabirov, M. Yu. Murashkin, R. Z. Valiev. Mater. Sci. Eng. 560 A, 1 (2013). Crossref
8. E. Avtokratova, O. Sitdikov, M. Markushev, M. Linderov, D. Merson, A. Vinogradov. Mater. Sci. Eng. 806 A, 140818 (2021). Crossref
9. E. Ma. JOM. 58.4, 49 (2006). Crossref
10. S. Krymskiy, O. Sitdikov, E. Avtokratova, M. Markushev. Trans. Nonferrous Met. Soc. China. 30, 14 (2020). Crossref
11. E. Avtokratova, O. Sitdikov, O. Latypova, M. Markushev. Facta Universitatis. Series: Mech. Eng. 18, 255 (2020). Crossref
12. S. V. Krymskiy, P. A. Nikulin, M. Yu. Murashkin,

M. V. Markushev. Lett. Mater. 1 (3), 167 (2011). (in Russian) Crossref
13. S. V. Krymskiy, D. K. Nikiforova, M. Yu. Murashkin, M. V. Markushev. Prosp. Mater. 12, 387 (2011). (in Russian)
14. M. V. Markushev, E. V. Avtokratova, S. V. Krymskiy, O. Sh. Sitdikov. J. Alloys Compd. 743, 773 (2018). Crossref
15. M. V. Markushev, E. V. Avtokratova, O. Sh. Sitdikov. Lett. Mater. 7 (4), 459 (2017). Crossref
16. L. F. Mondolfo. Structure and properties of aluminum alloys. Metallurgy, Moscow (1979) 640 p. (in Russian)
17. M. V. Markushev, E. V. Avtokratova, Yu. L. Burdastykh, S. V. Krimsky, O. Sh. Sitdikov. Lett. Mater. 10 (4), 517 (2020). (in Russian) Crossref
18. F. J. Humphreys, M. Hatherly. Recrystallization and Related Annealing Phenomena. Elsevier (2004) 658 p. Crossref
19. T. Sakai, A. Belyakov, R. Kaibyshev, H. Miura, J. J. Jonas. Progr. Mater. Sci. 60, 130 (2014). Crossref
20. I. G. Brodova, I. G. Shirinkina, A. N. Petrova. Lett. Mater. 1 (1), 32 (2011). (in Russian) Crossref
21. R. Z. Valiev, I. V. Aleksandrov. Bulk Nanostructured Metallic Materials: Production, Structure and Properties. Moscow, Akademkniga (2007) 398 p. (in Russian)
22. S. G. Alieva, M. B. Altman, S. M. Ambartsumyan et al. Promyshlennye aluminievye splavy. Moskva, Metallurgiya (1984) 528 p. (in Russian)
23. A. Deschamps, F. De Geuser, Z. Horita, S. Lee, G. Renou. Acta Mater. 66, 105 (2014). Crossref